Electrical Power and Energy Systems 154 (2023) 109471

Contents lists available at ScienceDirect

International Journal of Electrical Power and Energy Systems

journal homepage: www.elsevier.com/locate/ijepes

Transient current protection for transmission lines based on the Kalman filter measurement residual

Daniel Texidor Dantas [a], Jésus Anício de Oliveira Neto [b], Giovanni Manassero Junior [b,*]

[a] National Grid, National Grid House, Warwick Technology Park, Warwick, CV43 6DA, Warwickshire, United Kingdom
[b] Universidade de São Paulo, Avenida Professor Luciano Gualberto - Travessa 3, 158, São Paulo, 05508-010, São Paulo, Brazil

ARTICLE INFO

Keywords:
Power system protection
Power system relaying
Power transmission protection
Kalman filtering

ABSTRACT

This paper introduces a pilot protection method for two-terminal transmission lines based on the measurement residual of an extended Kalman filter designed to track alternate current signals. Transmission lines that interconnect generation plants to consumers are the primary equipment most susceptible to faults, and failing to isolate them correctly and promptly may lead to system collapse. In this context, the measurement residual allows for rapid fault identification and tripping. In addition, the proposed solution requires computing and communication resources typically available for pilot protection since it uses conventional sampling rates and has a low computational burden. This paper details the theory and application of the extended Kalman filter and the results of the proposed method when tested against different simulation scenarios. These scenarios were built on an extra-high voltage transmission system implemented in ATP/EMTP, varying fault impedance, inception angle, distance, phases involved, and fault type. It also presents a statistical analysis of these scenarios, including channel asymmetry, errors in the current transformers' conversion rate, and noise. Besides, it describes an analysis of the proposed method regarding current transformer saturation, high impedance faults, zero-crossing faults, external breaker opening, and power-swing. Finally, it compares the solution with other algorithms in the literature. The results indicate that the proposed solution is fast, accurate, secure, and dependable.

1. Introduction

Interconnected electrical power systems are susceptible to faults that need to be rapidly isolated to preserve power system stability, avoid equipment damage, and improve safety [1]. The isolation procedure comprises correct fault identification, communication delay, and the respective circuit breakers tripping. Reducing the necessary time to perform any of these actions enhances the system's dynamic performance during faults.

Nowadays, protection systems that detect faults in primary equipment rely on algorithms embedded in micro-processor-based devices that use the discrete Fourier transform (DFT) to calculate root mean square (RMS) values or phasor quantities of voltages and current signals. Then, these algorithms use these quantities as inputs of conventional protection functions. Therefore, they generally require at least one cycle of the fundamental frequency but must be fast while preserving security and dependability.

Overhead transmission lines (TLs) interconnect power plants to consumers and typically cover long distances. They are the equipment more susceptible to faults, which can occur due to contact with vegetation, fire, lightning, insulation failures, etc. Interconnected power systems are often made more resilient by enhancing, TLs' protection systems using pilot communication channels to improve isolation times. This reduces faults effects on the overall system. TLs' most common pilot protection functions are directional overcurrent, distance, and differential.

Directional overcurrent protection operation time can be relatively slow compared to the other two. Besides, it can present dependability and security failures, especially for close-in faults. Distance protection has limited fault coverage and is sensitive to changes in the impedance of the TL. It presents dependability and security failures for high-impedance faults, in-feed currents, heavy loading conditions, and also close-in faults. Both protection functions employ communication channels that exchange blocking or tripping signals to improve security, dependability, and tripping speed. On the other hand, differential protection is highly secure and dependable and usually provides correct and fast tripping. However, it is not immune to current transformer (CT) saturation, TL charging currents, and power swing [2], or communication delays [3,4], and [5].

* Corresponding author.
E-mail address: manassero@usp.br (G. Manassero Junior).

https://doi.org/10.1016/j.ijepes.2023.109471
Received 30 March 2022; Received in revised form 12 July 2023; Accepted 24 August 2023
Available online 5 September 2023

The literature shows that research topics related to pilot protection schemes for TLs focus on conceiving faster, more secure, and dependable protections. Usually, these algorithms lie in three main groups: frequency-domain, knowledge-based, or time-domain (or a combination of them).

Frequency-domain algorithms use phasor quantities of phase and symmetrical components of the voltages and current signals at the TL terminals, calculated using the discrete Fourier transform (DFT) that presents the disadvantage of requiring at least one cycle of these signals to calculate them correctly, to process the protection functions. Knowledge-based algorithms have been proposed in the literature to mitigate this problem and to cope with the issues that conventional pilot protection presents. However, their robustness depends on precisely modeling all abnormal conditions in the protected equipment to avoid jeopardizing security and dependability for actual faults. Time-domain methods use voltage and current signals in the discrete-time domain to build sets of equations, using linear and non-linear digital filters, usually faster than the DFT, to process the protection functions.

Concerning frequency-domain algorithms, Ref. [6] proposes an algorithm for longitudinal differential protection of TLs that is based on root mean square (RMS) values. Ref. [7] also presents a pilot protection method. It is based on the combination of the distance and differential protection functions that mitigates the effect of the fault impedance. The authors of [8] describe a differential scheme based on the α-plane that depends on measurements of voltage and current signals and uses the ratio of the current phasors associated with information about the phase angle between voltage and current at both TL ends.

Refs. [9,10], and [11] present knowledge-based algorithms that implement adaptive distance and differential protection schemes capable of coping with conventional current differential protection problems in TLs. Ref. [9] presents a distance protection function based on the concept of superimposed components of voltage and currents at both terminals of the TL. It can fastly discriminate between internal and external faults. However, the method depends on correct values for the TL quadrupole parameters, and it is based on frequency-domain values. The authors of [10] describe an adaptive current differential protection that improves the synchronization between intelligent electronic devices (IEDs), but it is based on current phasors. Ref. [11] uses continuous wavelet transform to improve the current differential protection method, extracting high-frequency information of the currents' signals. However, it requires a high sampling rate, 100 [kHz], therefore demanding a more sophisticate telecommunication infrastructure.

Time-domain algorithms can be divided into two subgroups. The first uses current and voltage samples, or their incremental quantities, and the second depends on current and voltage traveling waves (TWs). Both time-domain techniques present fast solutions, generally offering a considerable advantage regarding tripping times compared with conventional alternatives based on phasor estimation techniques.

Refs. [12–15] belong to the first group. While [12,14] investigate the use of active and reactive power entering and leaving the TL requiring voltage and current samples to assess its operating conditions correctly, Ref. [13] proposes the use of signed correlation criterion to evaluate the similarity between the signs of the phase current samples. On the other hand, Ref. [15] proposes using an incremental quantities strategy, but it requires higher sampling rates, in the order of tens of [kHz], and demands a more expensive telecommunication infrastructure.

Refs. [16,17] belong to the second group. Usually they need high sampling rates to determine the arrival times, polarity, and magnitude of the TWs to identify internal faults [17]. Besides, they also need complex algorithms to differentiate incident wave-fronts from reflected ones and usually present poor performance when faults initiate close to the voltage zero crossings. They also rely on sophisticated communication infrastructure to cope with the limited bandwidth of coupling capacitor voltage transformer (CCVT) or present approaches to simplify it [16].

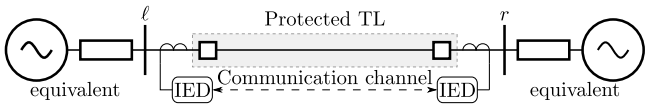

Fig. 1. System topology.

Ref. [18] proposes an algorithm that uses the fast Fourier transform (FFT) to extract the dc decaying component to observe its polarity at both line terminals. The authors also propose a decision-making trip algorithm that needs half a cycle to provide secure and dependable protection, making it slower than other similar algorithms [14].

1.1. Proposed method contributions

The manuscript presents the development, implementation, and tests of a time-domain transient current protection algorithm for TLs, based on information extracted from the measurement residual of current estimates from an extended Kalman filter (EKF). The proposed method can separate transient phenomena from the operating conditions and identify the faults within the protected TL.

To the best of the authors' knowledge, no protection method in the literature implements protection functions using only the measurement residual of EKFs.

The contribution proposed in the manuscript is a high-speed protection algorithm that uses the measurement residual of an EKF to determine the fault occurrence and that can embed IEDs with conventional sampling rates as low as 1 [kHz]. The proposed method is faster than typical differential protection functions implemented in these IEDs, presenting trip times in the same order of magnitude as TW protection. Distinctively from the latter, the proposed method does not use high-pass filtering. Therefore, it can detect zero-crossing faults.

Besides, since the proposed method runs with low sampling rates and uses only current signals at both line terminals, it is possible to employ it on standard 64 kbps communication channels [19]. Therefore, this paper intends to contribute to the time-domain protection research subject by presenting a cost-effective and fast protection function while preserving security and dependability.

1.2. Manuscript structure

The rest of the paper is structured as follows: Section 2 details the transient current protection method proposed by the authors regarding its theory and application; Section 3 describes necessary practical considerations for applying the technique; Section 4 presents the results of the proposed method when tested against different simulation scenarios of an extra-high voltage transmission system implemented in ATP/EMTP, varying fault impedance, inception angle, distance, phases involved, and fault type, as well as a statistical analysis of its performance with regards to CT saturation, communication delays, TL charging current and power swing, and; Section 5 concludes the paper.

2. Transient current protection method

The method proposed in this paper observes changes in the current signals at the TL terminals to determine whether there is an internal or external fault in the power system or if it is operating normally. To explain the detection strategy, one can consider the TL depicted in Fig. 1. In this figure, both CTs measure the current entering the protected circuit.

Faults in this system generate transient currents dependent on its electric characteristics, fault location, and inception angle. However,

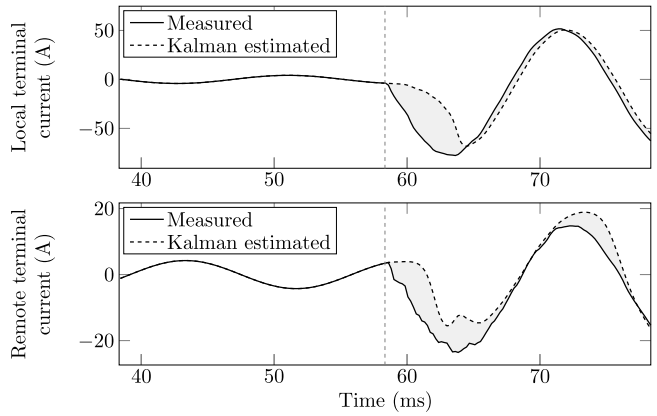

Fig. 2. Transient currents compared to estimated values using the EKF — Internal fault.

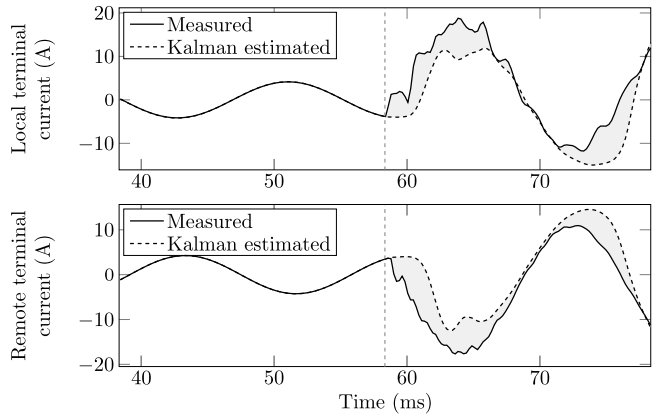

Fig. 3. Transient currents compared to estimated values using the EKF — External fault.

internal faults generate transient currents that differ from the pre-fault condition to the same polarity on both terminals, as depicted in Fig. 2. On the other hand, transient currents caused by external faults have different polarities when flowing through the protected TL, as illustrated in Fig. 3.

In this scenario, the proposed method uses a frequency tracking EKF [20] to estimate the time-domain pre-fault conditions. Whenever a transient event occurs, the measurement residual from the filter update stage corresponds to the desired transient information.

Many power system applications use Kalman filters (e.g., evaluation of harmonic distortion, minimization of measurement noise, and disturbance detection [20,21], and [22]). Nonlinear systems may use the extended variant of Kalman filters in many applications, like the one implemented in this paper. The proposed strategy uses the measurement residual of the EKF. It does not remove information from the transient signal since the measurement residual is the difference between the steady-state current model and the measured values. So, it preserves valuable information, unlike typical protection functions that rely on digital filters to extract information on the fundamental frequency or high-frequency transients.

Thus, the proposed method uses the extended Kalman filter to track pre-fault current signals and separate them from the measured ones. This filter can correctly track the current flow (i) in various scenarios, as described in the following sections. However, during abrupt current changes, the filter registers a measurement residual ($\tilde{i}$) related to its designed inability to track the transient currents instantaneously. Therefore, the difference between the EKF currents from the measured

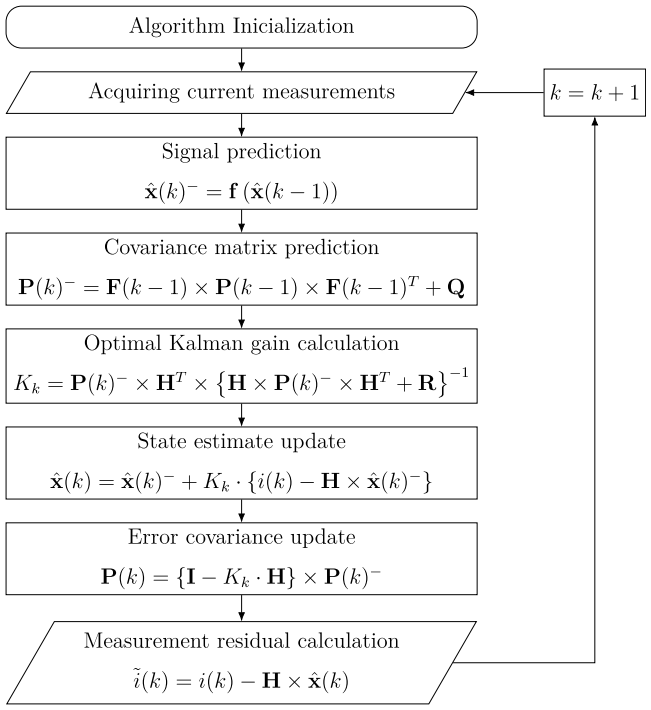

Fig. 4. EKF block diagram.

values produces a measurement residual that indicates the occurrence of transients.

The EKF continuously tracks the currents to estimate their subsequent measurements in this context. The authors implemented the filter as outlined in Fig. 4.

The proposed EKF uses a complex sinusoidal signal model based on Euler's formulation to describe the currents' behavior, as in

$$a \cdot \sin(k \cdot w \cdot T_s + \phi) = a \cdot \frac{e^{j\cdot(k\cdot w\cdot T_s+\phi)} - e^{j\cdot(-k\cdot w\cdot T_s-\phi)}}{2j} \tag{1}$$

where a is the amplitude of the sinusoidal signal, k is the kth sample, T_s is the complex sinusoidal signal sample period, w is its angular frequency, ϕ is its angle, and j is the imaginary unit. This paper adopts the complete three-state model used in [21,23], as in

$$\lambda = e^{j\cdot w\cdot T_s} \tag{2}$$

$$\beta(k) = a \cdot e^{j\cdot(k\cdot w\cdot T_s+\phi)} \tag{3}$$

$$\beta(k)^* = a \cdot e^{j\cdot(-k\cdot w\cdot T_s-\phi)} \tag{4}$$

Using this model to represent the power system allows for describing amplitude, phase, and frequency variations ($|\beta(k)|$, $\angle\beta(k)$, and $\angle\lambda$, respectively). Then, it is possible to express it in state space, as in

$$\begin{bmatrix} \lambda \\ \beta(k+1) \\ \beta(k+1)^* \end{bmatrix} = \begin{bmatrix} 1 & 0 & 0 \\ 0 & \lambda & 0 \\ 0 & 0 & \lambda^{-1} \end{bmatrix} \times \begin{bmatrix} \lambda \\ \beta(k) \\ \beta(k)^* \end{bmatrix} + \mathrm{w}(k) \tag{5}$$

where $\mathrm{w}(k)$ is the process noise. The signal measurement can be represented as in

$$i(k) = \begin{bmatrix} 0 & \frac{1}{2\cdot j} & \frac{1}{2\cdot j} \end{bmatrix} \times \begin{bmatrix} \lambda \\ \beta(k) \\ \beta(k)^* \end{bmatrix} + \mathrm{v}(k) \tag{6}$$

where $\mathrm{v}(k)$ is the measurement noise. The nonlinear process, as in (7) and (8), is the EKF model.

$$\mathbf{x}(k+1) = \mathbf{f}(\mathbf{x}(k)) + \mathrm{w}(k) \tag{7}$$

$$i(k+1) = \mathbf{H} \times \mathbf{x}(k+1) + \mathrm{v}(k) \tag{8}$$

where $x(k)$ is the kth sample of the intermediate state, **f** is the state transition model, and **H** is the observation model. The state transition model is updated using only the previous state information without inputs from the process. The state transition and observation models are, respectively,

$$\mathbf{f}(\mathbf{x}(k)) = \begin{bmatrix} \lambda & \lambda \cdot \beta(k) & \lambda^{-1} \cdot \beta(k)^* \end{bmatrix}^T \tag{9}$$

$$\mathbf{H} = \begin{bmatrix} 0 & -0.5 \cdot j & 0.5 \cdot j \end{bmatrix} \tag{10}$$

It is possible to estimate the complex sinusoidal signal from the system's linearization and with the use of a recursive nonlinear filter [24]. The system's linearization along its trajectory is calculated using the covariance matrix (**P**), and the estimation step is divided into two: prediction and update.

2.1. Prediction

The nonlinear system output prediction at instant $t(k)$, given the state estimation at instant $t(k-1)$, is illustrated in the "Signal prediction" block depicted in Fig. 4. Where the signal "$^-$" represents the *a priori* estimate given the measurements of the previous sample (i.e. $\hat{\mathbf{x}}(k)^-$ is predicted considering the updated measurement from sample $k-1$).

The covariance matrix ($\mathbf{P}^-$) is predicted using the Jacobian matrix (**F**) and the process noise covariance (**Q**), as illustrated in the "Covariance matrix prediction" block depicted in Fig. 4, where

$$\mathbf{F}(k-1) = \left| \frac{\partial \mathbf{f}(\mathbf{x}(k-1))}{\partial \mathbf{x}(k)} \right|_{\mathbf{x}=\hat{\mathbf{x}}} = \begin{bmatrix} 1 & 0 & 0 \\ \hat{u}(k-1) & \lambda & 0 \\ \dfrac{-\hat{u}(k-1)^*}{\lambda^2} & 0 & \dfrac{1}{\lambda} \end{bmatrix} \tag{11}$$

Considerations regarding the selection of the process noise covariance are presented in Section 3.

2.2. Update

The *a priori* estimate is corrected, as illustrated in the "State estimate update" block depicted in Fig. 4, where $i(k)$ is the current measurement at instant $t(k)$. To perform the update, it is necessary to calculate the optimal value of the Kalman filter gain (K_k) as illustrated in the "Optimal Kalman gain calculation" block depicted in Fig. 4, where (**R**) is the observation noise covariance.

After updating the *a priori* estimate, the error covariance matrix is also updated , as illustrated in the "Error covariance update" block depicted in Fig. 4.

Finally, the measurement-residual calculation is performed as shown in Fig. 4, where $\tilde{i}(k)$ is the measurement residual. This variable is used in the proposed transient current protection algorithm.

Considerations regarding the process and observation noises are detailed in Section 3.

2.3. Fault detection

As previously mentioned, the authors propose using the measurement residual, calculated on the update step of every iteration of the EKF, to evaluate if a transient current signal represents an internal fault.

To improve security and dependability, the measurement residual is discrete-time integrated and then used to evaluate the transients' effect on the currents of each TL terminal. The authors chose to implement a rectangular discrete-time integration, as in (12) and (13), since it provides satisfactory results while being simple.

$$A_{\ell\phi}(k) = \sum_{a=k-n+1}^{k} \tilde{i}_{\ell\phi}(a) \cdot \Delta t \tag{12}$$

$$A_{r\phi}(k) = \sum_{a=k-n+1}^{k} \tilde{i}_{r\phi}(a) \cdot \Delta t \tag{13}$$

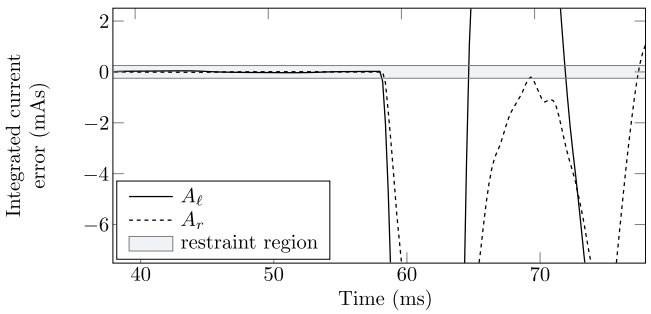

Fig. 5. Behavior of A_ℓ and A_r during an internal fault.

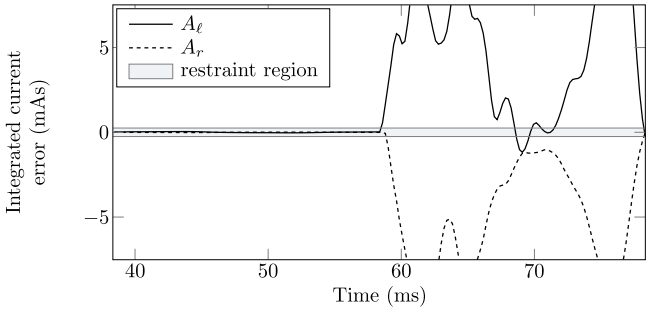

Fig. 6. Behavior of A_ℓ and A_r during an external fault.

where $A_{\ell\phi}(k)$ and $A_{r\phi}(k)$ are the discrete-time integrated measurement residuals of the last n current samples from phase ϕ, with a sampling period of Δt, at the local end remote terminals, respectively.

First, the integrated measurement residual is compared to a minimum threshold on both terminals, as in (14) and (15), to determine if it represents an event with a transient level significant enough to indicate an internal fault.

$$\left|A_{\ell\phi}\right| > A_{min} \tag{14}$$

$$\left|A_{r\phi}\right| > A_{min} \tag{15}$$

After confirming that both discrete-time integrated measurement residuals are greater than the thresholds, the algorithm verify if their polarities are the same, as in

$$A_{\ell\phi} \cdot A_{r\phi} > 0 \tag{16}$$

If the conditions presented in (14) and (15) are met, the algorithm indicates the presence of an internal or external fault in the transmission system. The discrimination between internal and external faults uses the discrete-time integrated measurement residuals, as in (16). During an internal fault, $A_{\ell\phi}$ and $A_{r\phi}$ exit the restraint region, established between $-A_{min}$ and $+A_{min}$, in the same direction. Both are negative in the example depicted in Fig. 5. Conversely, during an external fault, those quantities leave the restraint region through different directions, exemplified in Fig. 6.

Digital implementation, as well as the protection settings, are described in Section 3.

3. Implementation

The proposed algorithm is phase segregated, as customary protection implementations. Therefore, it calculates the integrated measurement residual for all TL phases in each terminal (ℓ or r).

One consideration is that if an external fault occurs during the accommodation of the EKF, the algorithm may present security failures. This is evident when analyzing the 69th ms of Fig. 6. During this transient caused by an external fault, both $A_{\ell\phi}$ and $A_{r\phi}$ are below

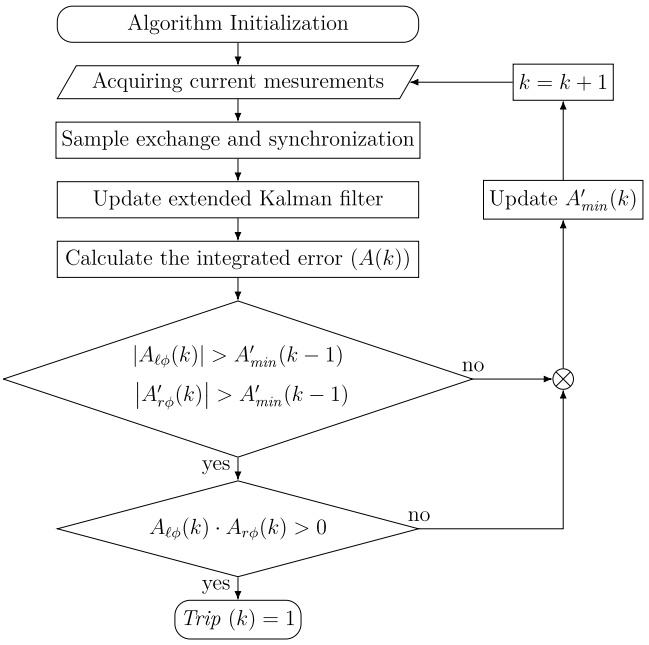

Fig. 7. Protection algorithm block diagram.

$-A_{min}$. Therefore, whenever $A_{\ell\phi}$ and $A_{r\phi}$ leave the restraint region, the proposed method should trip or increase the restraint region, similar to conventional differential protection, depending on whether those quantities go through the same boundary ($-A_{min}$ and A_{min}). Fig. 7 depicts the algorithm's behavior.

Therefore, the algorithm uses an adaptive restraint region to avoid security failures at the cost of sensitivity. The adapted strategy consists of using an adaptive A'_{min}, as in

$$A'_{min}(k) = \max\left\{\begin{bmatrix} A_{min} \\ A_{\ell\phi}(k) \cdot A_{r\phi}(k) < 0 \ : \ \min\left\{|A_{\ell\phi}(k)|, |A_{r\phi}(k)|\right\} \\ A'_{min}(k-1) \cdot (1-\rho) \cdot \Delta t \end{bmatrix}\right\} \quad (17)$$

where the first line determines a minimum threshold (A_{min}); the second expresses the maximum transient in the respective phases, which increases the restraint region to avoid external faults to provoke security failures; and the third decreases the threshold by the rate of change ρ (expressed in % over ms) to avoid dependability failures. The choice to update of the restraint region based on the minimum residual value prioritizes dependability and was made because it did not result in any security maloperations. Nonetheless, external events will cause the adaptive restraint region to reduce sensitivity. Therefore, it is recommend to use backup protection functions (as per common practice in the industry).

3.1. Settings

The protection performance depends on the EKF parameters, A_{min}, ρ, and integration time. The observation and process noise covariance values used in this paper are 3% and 1.5×10^{-6}%, respectively. The first value represents a signal-to-noise ratio of 15 dB of the measured current signals. The authors chose the latter to enable the algorithms to track power swings, as explored in session 4.8.

The authors set the minimum threshold (A_{min}) as 20% of the TL rated current multiplied by the sampling period. High impedance faults in transmission systems create current steps that can be detected using this threshold. The authors set the rate of change value (ρ) as −1% per ms, and, finally, the discrete-time integration window is close to 1 ms, which is twice the traveling time of the TL used in the simulation scenarios.

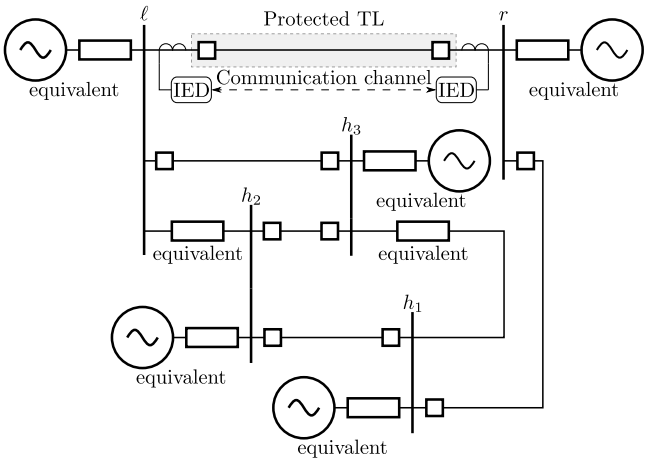

Fig. 8. System topology [25].

4. Dynamic studies

The authors submitted the proposed protection method to challenging simulation scenarios that emulate actual protection case studies to describe better the principles involved. The method's response to these scenarios illustrates its working mechanism, and the figures that depict the currents' signals and the behavior of the proposed Kalman estimator assist in its unveiling. These challenging scenarios are:

- internal and external faults with and without channel asymmetry (current samples misalignment), errors in the CT conversion rate, and noise (Section 4.3);
- CT saturation (Section 4.4);
- high impedance internal and external faults, up to 500 Ω (Section 4.5);
- zero crossing faults (Section 4.6);
- external breaker opening (Section 4.7); and
- power swing (Section 4.8)

These case studies allow the authors to determine the proposed method's behavior and validate its security and dependability. They are essential for testing conventional and innovative protection algorithms and systems because they can accurately replicate challenging conditions that usually compromise them. This helps ensure that algorithms and systems are functioning correctly and can detect faults and initiate protective actions as intended, reducing the risk of power system security and dependability failures and improving overall system reliability.

Besides detailing the algorithm's response to these simulation scenarios, the authors present a comparison with other methods proposed in the literature, in Section 4.10.

4.1. Transmission system

The authors tested the proposed protection algorithm against simulation scenarios built on Brazilian transmission systems (except the results provided in Section 4.8) using the software ATP/EMTP. The authors chose to present the algorithm's performance regarding the 500 kV, 5-bus transmission system depicted in Fig. 8. This system is located southeast of Rio de Janeiro and offers realistic transients while preserving readability. Table 1 shows the fault levels of all buses.

The TLs were modeled in ATP/EMTP using a frequency-dependent distributed parameters model [26] in the *line constants* ATP/EMTP

Table 1
Fault levels in each bus — MVA.

Bus	Single phase	Three phase
ℓ	9361.1 ∠88.75°	7804.0∠88.57°
r	–	1538.7 ∠90°
h_1	3593.8 ∠85.96°	3798.2∠87.34°
h_2	7285.6∠85.86°	8385.3∠87.07°
h_3	4198.6∠87.08°	3363.4∠86.61°

Table 2
Transient events applied to the system.

Event	Inception angle	R_f [Ω]	Number of Simulations
ABC faults	0° 45° 90°	0, 1, 5	144 (108[a])
AN faults		0, 10, 50, 100, 150, 200, 250, 300, 400, 500	480 (360[a])
BC faults BCN faults		0, 2, 10	288 (216[a])
Breaker opening	–	–	8

[a]Internal faults.

supporting routine. There are four-bundled conductors for each phase (Rail 954 MCM ACSR conductors) and two Alumoweld cables (diameter of 9.78 mm) for the overhead ground wires. The external phases' vertical bundle height at the tower is 35.64 m, while the central phase vertical bundle height at the tower is 41.04 m. The phase conductors sag is 26.14 m, and the horizontal distance between the center of each bundle of conductors is 10.6 m. Both ground wires' vertical bundle height at the tower is 46.34 m. The ground wires' sag is 11.49 m, and the horizontal distance between both ground wires is 15.4 m. Besides, soil resistivity was 1000 Ω m. The CTs in both buses ℓ and r have a 1200:5 relation and a saturation characteristic modeled according to [27]. They measure the currents entering the protected TL.

4.2. Automated testing

The authors created an automated test structure to evaluate these simulation scenarios using the system depicted in Fig. 8. The faults were applied to the protected TL, adjacent buses, and adjacent TLs. Breaker opening and closing maneuvers also were run across the system.

The authors evaluated the proposed method with two sampling rates, 80 samples per cycle (as expected for protection sampled values in the IEC 61850) and 20 samples per cycle. The authors chose the latter to evaluate the possibility of using a single 64 kbps pilot connection channel described in [4]. The simulations that explore all the challenging conditions, except the power swing, were run based on the previously described system using ATP/EMTP. These simulations have a 10 μs integration step, and the stored digital signals were re-sampled using a (3rd order lowpass Butterworth filter with 3 dB of attenuation on the bandpass frequency of 1/3 of the sampling frequency and over 40 dB of attenuation in the stopband frequency of 1/2 of the sampling frequency). The authors implemented the filter and protection algorithms in GNU Octave.

The authors used the 920 scenarios described in Table 2 to perform 1840 ATP/EMTP simulations. The number was doubled because all cases were also simulated with an increased burden on the local CTs to test the algorithms' tolerance to saturation. Of the 920 scenarios, 684 cases corresponded to internal faults.

4.3. Algorithm robustness analysis

The proposed algorithm correctly identified all internal faults and did not present security errors for external faults. To further test the algorithm, the authors deliberately introduced three sources of error: sample misalignment of 0.2 ms (channel asymmetry), CT precision error of 10%, and noise (a signal-to-noise of approximately 40 dB implemented as a sampling error considering three imprecise bits on a 10-bit analog-to-digital converter).

Table 3
Detailed trip times.

Samples per cycle	Trip times [ms]		
	μ	max	min
80	0.702	3.230	0.257
80 with CT sat.	0.701	3.230	0.257
20	1.490	4.070	1.307
20 with CT sat.	1.491	4.070	1.307

Maximum trip times occur for high-impedance faults near the weaker TL terminal.

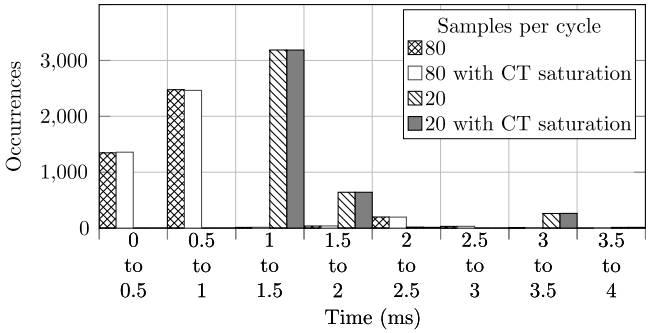

Fig. 9. Trip time distribution.

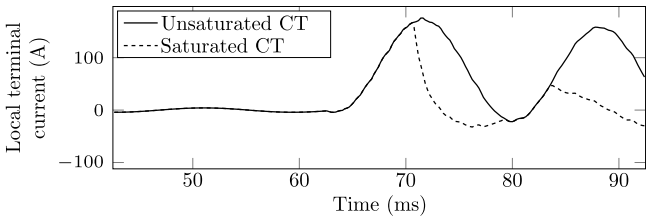

Fig. 10. Comparison between the same case with and without CT saturation on one of the line's terminal.

The fastest recorded trip time is 0.257 ms. Table 3 presents the average trip times (μ), maximum (max), and minimum (min) trip times. Fig. 9 depicts the trip time distribution for the different sampling rates, with and without current samples misalignment, errors in the CT conversion rate, and noise. It is interesting to notice that higher sampling rates improve the fault detection times from an average trip time of 1.49 ms (20 samples per cycle) to 0.70 ms when using 80 samples per cycle. Most of this difference can be attributed to the delay introduced by the antialiasing filter.

4.4. Current transformer saturation

The authors repeated the same simulations but using a higher burden impedance on the CT secondary, as described in [27] and illustrated in Fig. 10. The proposed algorithm correctly classified the faults as internal within 4.07 ms, which means that the trip decision is made before CT saturation becomes significant. It presented virtually the same results with the unsaturated CTs. Besides, the algorithm did not show any security or dependability failures, and the trip time distributions did not have significant changes, as one can notice in Fig. 9.

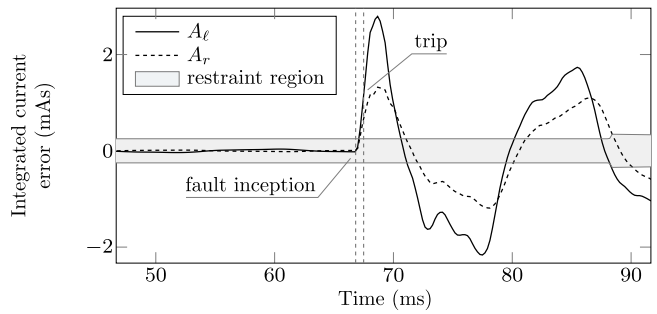

Fig. 11. High resistance fault — Behavior of A_ℓ and A_r.

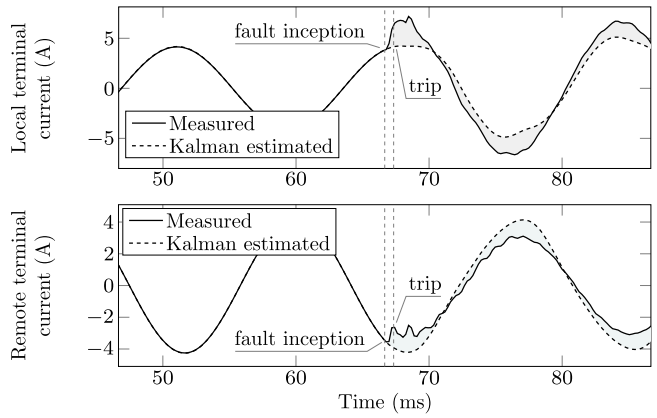

Fig. 12. High resistance fault — Transient currents compared to estimated values using the EKF.

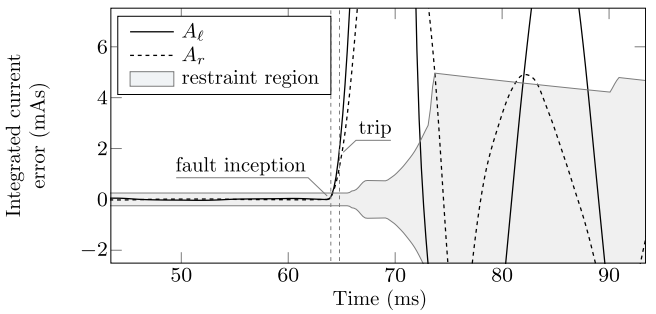

Fig. 13. Zero-crossing fault — Behavior of A_ℓ and A_r.

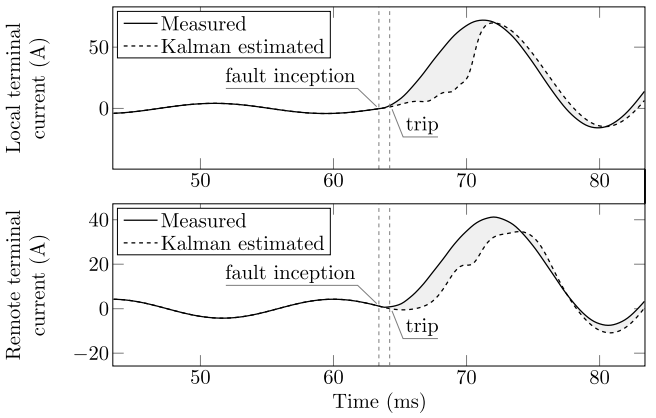

Fig. 14. Zero-crossing fault — Transient currents compared to estimated values using the EKF.

4.5. High impedance internal and external faults

The proposed protection can identify high resistance faults because even minor disturbances generate transients consistent with the described phenomena. The 500 Ω internal fault, depicted in Figs. 11 and 12, was detected at 0.743 ms after fault inception. This detection was made using the same settings as described in Section 4.2. It is interesting to notice that this case exemplifies an outfeed condition, which does not negatively interfere with the protection algorithm.

4.6. Zero-crossing faults

The proposed protection does not use traveling waves to detect faults. Therefore, it can identify zero-crossing faults. Even though these events are unlikely to happen in practical power systems, evaluating such faults indicates that the proposed algorithm is dependable, even for low incidence angles. The fault depicted in Figs. 13 and 14 is a zero-crossing fault, and the proposed protection function was able to detect it within 0.847 ms after fault inception.

Using the measurement residual from the EKF estimation avoids removing fundamental frequency components from the fault current. This strategy allows for reliable fault identification, even if no high-frequency elements are generated. Fig. 14 depicts a fault with few high-frequency components in its wavefront, which is identified as an internal event. Despite this example, it is worth mentioning that some high impedance faults ($R > 100$ Ω), with low inception voltages, were the slowest faults to identify.

4.7. External breaker opening

Opening or closing circuit breakers may interfere with the response of protection functions (e.g., distance protection and traveling waves).

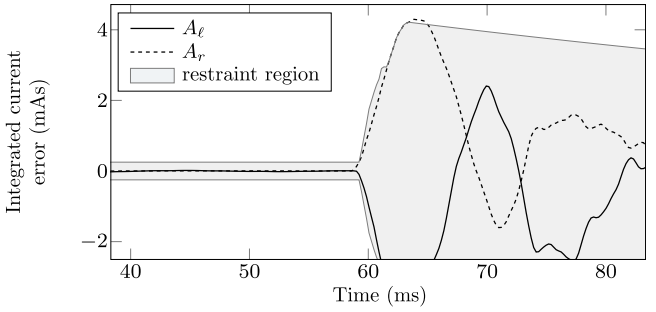

Fig. 15. Maneuver of adjacent circuit breaker — Behavior of A_ℓ and A_r.

External events may result in the opening of circuit breakers not related to the protected equipment. However, they create incremental currents with opposite polarities, similar to external faults. For the tested cases, the proposed algorithm regarded these as external events. An example of transients with measurement residual in opposing directions caused by opening a circuit breaker adjacent to the protected TL is depicted in Figs. 15 and 16.

4.8. Power swing

The authors used the power swing simulation from [28] as a base to study a realistic voltage and frequency oscillation (adapted example from Fig. 7.8 of this reference) to evaluate the behavior of the proposed algorithm during frequency fluctuations. The simulation scenario consists of two series-connected double-circuit TLs that integrate an equivalent synchronous generator to an infinite bus.

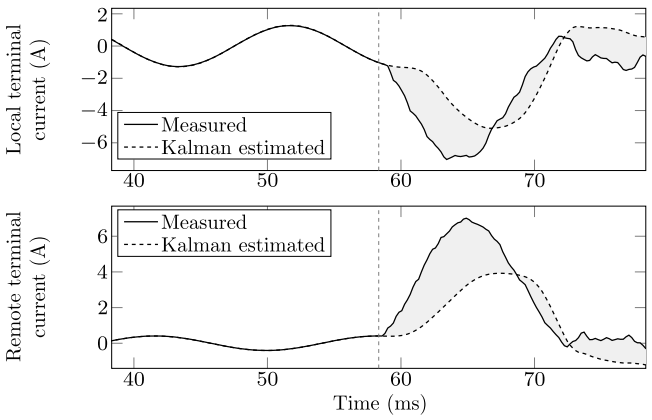

Fig. 16. Maneuver of adjacent circuit breaker — Transient currents compared to estimated values using the EKF.

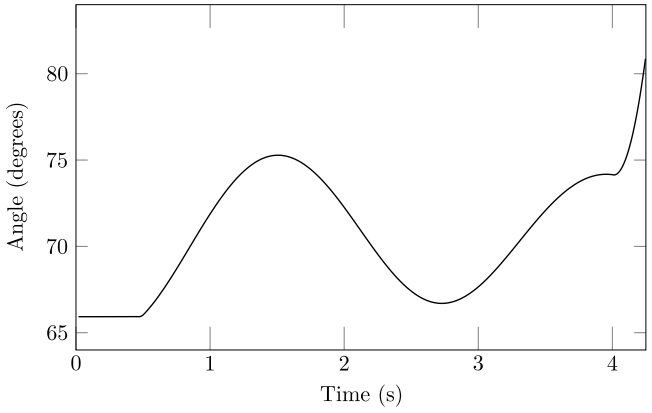

Fig. 17. Power swing generated by external event followed by internal fault — Angle difference between sources during the simulation.

The simulation consists of a three-phase fault at the parallel TL, connected to the generator, that starts at approximately 460 ms after the simulation begins and that is correctly isolated at around 500 ms, resulting in severe power swings. Then, a second three-phase fault starts, now at the protected transmission line which is also connected to the generator, starts approximately 4 s after the simulation begins.

This scenario produced the relative angular position depicted in Fig. 17 and the protection behavior described in Fig. 18.

The proposed algorithm did not trip during the three-phase fault at the parallel TL, nor during the power swing. After the inception of the internal fault, the algorithm operated as expected. Therefore, one can notice that the proposed method can differ internal faults from external events (e.g. external faults, power swings, etc.).

4.9. Hardware requirements

The proposed EKF, with execution sequence optimization, requires mostly multiplication and additions of 3×3 matrices. To obtain the Kalman gain (Fig. 4), calculating the internal elements before the inversion reduces the costly operation to a 1×1 matrix inversion (i.e., a complex number inversion), thus reducing the computational burden. This EKF application requires 505 floating-point operations for each new sample in one of the current channels. In the case of a three-phase system being sampled at 5 kHz (circa 80 samples per cycle), 15 million floating point operations per second (MFLOPS) would need

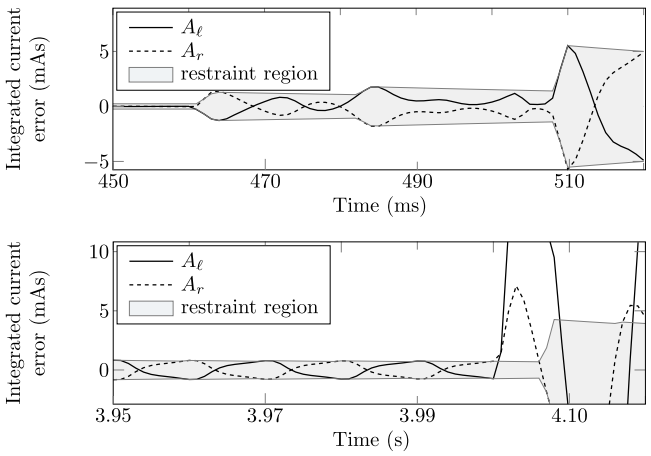

Fig. 18. Power swing generated by external event followed by internal fault — Behavior of A_ℓ and A_r.

to be allocated to calculate the six current channels. For reference, processors of circa 80 MFLOPS were used in conventional IEDs more than fifteen years ago.

Regarding communication requirements, the algorithm needs to transmit current data for each one of the 3 phases at 20 samples per 60 Hz cycle. Assuming 8 bit words per sample, the required data rate is 28.8 kbps. The low data bandwidth requirement makes it possible for this protection to rely on a single 64 bit channels, the minimal standard requirement for modern pilot protection, as specified in [19].

4.10. Operating times comparison

Table 4 presents a comparison between the proposed method and pilot protections presented in the in Refs. [14,15,29,30], and [31]. The data presented in Table 4 indicate that the proposed method presents shorter operating times when compared to all the other methods.

The operating times presented in this Table consider the algorithms processing and decision making times without considering communication delays between the TLs terminals, which would impact equally all of them. According to the IEEE standard [4] the time delay includes IED interface delay (1 to 5 ms), fiber optic propagation delay (5 μs/km), and substation multiplexer delay (0.4 ms). Therefore, 6 ms should be added to all the results of all the methods presented in Table 4 to contemplate for the communication delay.

The method presented in [14] uses voltage and current samples, while the method presented in [15] uses a sampling frequency of 10 kHz, which is twice the sampling frequency of the proposed method.

In addition, the method presented in [29] also has operating times higher than the proposed algorithm, and it requires special hardware and communication infrastructure, making the solution less cost-effective than the proposed one, since it uses the concept of traveling waves and needs a sampling frequency much higher. Besides, it will not trip when faults initiate close to the voltage zero crossings.

The algorithms presented in [30] have higher tripping times than the proposed method, and also use voltage and current samples. Besides, the authors state that they intentionally biased their algorithms for speed and security instead of dependability. Therefore, these algorithms need dependable, phasor-based protection operating in parallel, delaying even more the average operating times.

Finally, the algorithm presented in [31] present higher tripping times and use a statistical approach that must be fine tunned to produce secure, dependable and fast operating times.

Table 4
Operating times comparison.

Algorithm:	Proposed	[14]	[15]	[29]	[30]	[31]
Average trip time (ms):	0.7[b] and 1.5[c]	10.9	7	1.4	2 and 4[a]	6.6[b]
Sampling frequency (kHz):	4.8 and 1	2	25	1000	1000	4.8

[a]Directional power and distance, respectively.
[b]Sampling frequency of 4.8 kHz.
[c]Sampling frequency of 1.0 kHz.

5. Conclusion

The transient current protection algorithm proposed in this paper consists of an algorithm that can extract transient information from the currents measured at the line terminals. The algorithm uses the extended Kalman filter to model the pre-fault currents, making it possible to separate them from the faulty ones while preserving all remaining information. This procedure allows for reliable identification of fault events, even for zero-crossing faults.

The transient current protection described in this paper presented trip times under 1.5 ms for over 93% of the cases (the worst-case was detected within 4.07 ms using a sampling rate of 1.2 kHz). Therefore, the proposed alternative is among the fastest protections available. It is also cost-effective because it relies on typical protection hardware and communication infrastructures readily available in substations.

The results presented in the paper suggest that the proposed method is fast, dependable, and secure for all types of faults, considering ideal and critical fault conditions. To corroborate this statement, the authors presented the algorithm's behavior under ideal circumstances, and also high impedance faults, zero-crossing faults, CT saturation for external events, and power swings. Besides, the authors investigated the algorithm's behavior when dealing with noisy signals, harmonic content, and samples' misalignment and the results indicate that it preserved its behavior.

CRediT authorship contribution statement

Daniel Texidor Dantas: Conceptualization, Methodology, Software, Validation, Formal analysis, Investigation, Writing – original draft, Writing – review & editing. **Jésus Anício de Oliveira Neto:** Conceptualization, Methodology, Software, Validation, Formal analysis, Investigation, Writing – original draft. **Giovanni Manassero Junior:** Conceptualization, Methodology, Validation, Formal analysis, Investigation, Writing – original draft, Writing – review & editing, Supervision, Funding acquisition.

Declaration of competing interest

The authors declare that they have no known competing financial interests or personal relationships that could have appeared to influence the work reported in this paper.

Data availability

Data will be made available on request.

Acknowledgments

This work was supported in part by the Coordenação de Aperfeiçoamento de Pessoal de Nível Superior – Brasil (CAPES) – Finance Code 001.

References

[1] Zubic S, Gajic Z, Kralj D. Line protection operate time: How fast shall it be? IEEE Access 2021;9:75608–16.
[2] Anderson PM, Henville C, Rifaat R, Johnson B, Meliopoulos S. Power system protection. Hoboken, Estados Unidos: John Wiley & Sons; 2022.
[3] Albi P, Sánchez JC, Rodríguez C, Fernández A, Ramos D, Caballero A, et al. Process bus interoperability under IEC 61869-9 differential protection (87L) scheme with one conventional end. In: CIGRE 2018 Paris session papers & proceedings. 2018, p. 1–10.
[4] PE/PSRCC - Power System relaying and control, std C37.243-2015 - guide for application of digital line current differential relays using digital communication, standard. Institute of Electrical and Electronics Engineers; 2015.
[5] Crossley PA, Guo H, Ma Z. Time synchronization for transmission substations using GPS and IEEE 1588. CSEE J Power Energy Syst 2016;2(3):91–9.
[6] Rajić T, Stojanović Z. An algorithm for longitudinal differential protection of transmission lines. Int J Electr Power Energy Syst 2018;94:276–86.
[7] Ghorbani A, Mehrjerdi H, Al-Emadi NA. Distance-differential protection of transmission lines connected to wind farms. Int J Electr Power Energy Syst 2017;89:11–8.
[8] Sarangi S, Pradhan AK. Adaptive α-plane line differential protection. IET Gener Transm Distrib 2017;11(10):2468–77.
[9] Khoshbouy M, Yazdaninejadi A, Bolandi TG. Transmission line adaptive protection scheme: A new fault detection approach based on pilot superimposed impedance. Int J Electr Power Energy Syst 2022;137:107826.
[10] Zhou C, Zou G, Du X, Zang L. Adaptive current differential protection for active distribution network considering time synchronization error. Int J Electr Power Energy Syst 2022;140:108085.
[11] AsghariGovar S, Seyedi H. Adaptive CWT-based transmission line differential protection scheme considering cross-country faults and CT saturation. IET Gener Transm Distrib 2016;10(9):2035–41.
[12] Ma J, Ma R, Li J, Xu Y. A pilot protection method for the wind farm transmission line based on interaction power difference. Int J Electr Power Energy Syst 2023;147:108856.
[13] Saber A, Shaaban M, Zeineldin H. A new differential protection algorithm for transmission lines connected to large-scale wind farms. Int J Electr Power Energy Syst 2022;141:108220.
[14] Dantas DT, Pellini EL, Manassero Jr G. Time-domain differential protection method applied to transmission lines. IEEE Trans Power Deliv 2018;33(6):2634–42.
[15] Lei A, Dong X, Terzija V. An ultra-high-speed directional relay based on correlation of incremental quantities. IEEE Trans Power Deliv 2018;33(6):2726–35.
[16] Lei A, Dong X, Shi S, Wang B, Terzija V. Equivalent traveling waves based current differential protection of EHV/UHV transmission lines. Int J Electr Power Energy Syst 2018;97:282–9.
[17] Tang L, Dong X, Luo S, Shi S, Wang B. A new differential protection of transmission line based on equivalent travelling wave. IEEE Trans Power Deliv 2017;32(3):1359–69.
[18] Adharapurapu HL, Bhimasingu R. A novel algorithm for improving the differential protection of power transmission system. Electr Power Syst Res 2020;181:106183.
[19] PE/PSCC - power system communications and cybersecurity, ieee std C37.94-2017 (revision of IEEE std C37.94-2002) – IEEE standard for N times 64 kbps optical fiber interfaces between teleprotection and multiplexer equipment, standard. Institute of Electrical and Electronics Engineers; 2017.
[20] Neto JAO, Sartori CAF, Junior GM. Fault location in overhead transmission lines based on magnetic signatures and on the extended Kalman filter. IEEE Access 2021;9:15259–70.
[21] Dash PK, Jena R, Panda G, Routray A. An extended complex Kalman filter for frequency measurement of distorted signals. IEEE Trans Instrum Meas 2000;49(4):746–53.
[22] Girgis AA, Makram EB. Application of adaptive Kalman filtering in fault classification, distance protection, and fault location using microprocessors. IEEE Trans Power Syst 1988;3(1):301–9.
[23] Nishiyama K. A nonlinear filter for estimating a sinusoidal signal and its parameters in white noise: On the case of a single sinusoid. IEEE Trans Signal Process 1997;45(4):970–81.
[24] Kalman RE. A new approach to linear filtering and prediction problems. J Fluids Eng 1960;82(1):35–45.
[25] Dantas DT. Algoritmos de proteção diferencial no domínio do tempo baseados em energia e potência reativa [Ph.D. thesis], Escola Politécnica da Universidade de São Paulo; 2019.

[26] Marti JR. Accurate modelling of frequency-dependent transmission lines in electromagnetic transient simulations. IEEE Trans Power Appar Syst 1982;1(PAS-101):147–57.
[27] Folkers R. Determine current transformer suitability using EMTP models. In: 26th Annual western protective relay conference. 1999, p. 1–47.
[28] Haginomori E. Applied ATP-EMTP to highly-sophisticated electric power systems. Japanese ATP User Group (JAUG); 2003.
[29] Lopes FV, Ribeiro JPG, Leite EJS, Silva KM. Parametric analysis of the traveling wave-based differential protection TW87. J Eng 2018;2018(15):1297–302.
[30] Schweitzer E, Kasztenny B, Mynam M, Guzmán A, Skendzic V. New time-domain line protection principles and implementation. In: 13th International conference on developments in power system protection. 2016, p. 1–7.
[31] Tiferes RR, Manassero Junior G. Time-domain differential protection of transmission lines based on bayesian inference. IEEE Trans Power Deliv 2021;99:1–10.